THE 1988 YELLOWSTONE FIRES OBSERVED BY IMAGING RADARS

Eric Rignot[1], Don G. Despain[2], and Francesco Holecz[1]

Jet Propulsion Laboratory, California Institute of Technology,
4800 Oak Grove Drive, Pasadena CA 91109-8099

[1]Greater Yellowstone Field Station, Montana State University, Bozeman, MT 59717
[2]U. S. Geological Survey, Midcontinent Ecological Research Center
E-mail: ddespain@montana.edu

ABSTRACT

In 1988, nearly half a million hectares of forest burned in the Greater Yellowstone Area. Six years later, the burned areas were still visible in the dual-polarization radar images acquired by the Spaceborne Imaging Radar C (SIR-C) at both C- (5.6 cm wavelength) and L-band (24 cm) frequency. The data were georeferenced, rectified and calibrated using a digital topographic model of the park, and residual variations in radar backscatter were removed using an empirical correction. Burned areas were mapped using a supervised Bayesian classifier. The SIR-C classification was compared to 10 km x 10 km plots of visually interpreted aerial photos from 1988, a Landsat TM classification from 1988, and airborne radar data collected in 1989 and 1994 by the NASA/JPL AIRSAR instrument. The results show that the SIR-C data separate burn from non-burn with 78% accuracy and distinguish canopy burn from mixed burn. Canopy burn is in places overestimated but comparison with the AIRSAR data suggest that part of the forest at the edge of the fires died in subsequent years and holds less moisture. Vigorous forest regeneration is detected by the SIR-C data. These results illustrate imaging radar's abilities to survey large areas affected by wildfires, independent of cloud cover and smoke, and provide information on forest re-growth in the years following disturbances in terms of vegetation structure, woody biomass, and moisture levels.

INTRODUCTION

In 1988, Yellowstone National Park was affected by one of the largest complexes of wildland fires in the Northern Rocky Mountains in the last 50 years (Christensen et al., 1989). The fires attracted intensive media attention and deep public concern. Because they were so extensive and provided a unique opportunity to study forest regeneration, the 1988 fires also generated considerable scientific interest. Although they were vast, the fires were not at all unprecedented (Romme and Despain, 1989a and b). The unusual extent of the 1988 fires was the consequence of extreme drought and persistent high winds on the Yellowstone Plateau in the summer of 1988, combined with the presence of an extensive cover of highly flammable old-growth forests that had developed undisturbed since the early 1700's (Romme and Despain, 1989a and b).

Several post-fire studies estimated how much of Yellowstone was burned by the fire, the intensity of the fire, and the distribution of the burns (Despain et al., 1989; Rothermel et al., 1994). The results revealed a complex mosaic of completely burned areas (canopy burn), forest stands with various degrees of burn (mixed burn), areas of surface burn under unburned canopies (surface burn), and spatial scales ranging from a few meters to several kilometers. In canopy burn, the fire consumed all the needles and some small twigs of the trees and sapling crowns, ignited and consumed the litter, dry duff and rotten logs on the forest floor, consumed dead branches and tree boles less than 8-10 cm diameter, and charred the outside few cm of both standing and fallen dead trees (Despain et al., 1996). In mixed burn, the fire consumed the crowns of some trees, merely scorched the crowns of others or damaged trees that would die over the next three years. In surface burn, the fire crept around on the ground burning only patches of duff and rotten logs (Despain et al., 1989).

Two of the most important questions asked during the fire were: how much land has burned and where were the perimeters of the different fires at the end of each burning period? Answering those questions was difficult because ground surveying was risky and optical imagery could not be used through the smoke, especially in those areas where smoke from one fire obscured another fire. Infrared sensors were utilized at night over the most critical areas but only when they were not needed on fires with higher priority. Infrared images are difficult to interpret and rectify to maps because they rely on temperature differences rather than spatially-specific signatures. They only record hot spots along the most recently burned fire fronts. Estimates

of burned area varied widely depending on the definition of burned area and the uncertainty in the means of measuring it. The biggest problem eventually became the sheer magnitude of the fires which rendered airborne sensors impractical or of limited scope.

Imaging radar could provide a useful complement to these techniques because it can provide high-resolution imagery of burned areas, independent of cloud cover, smoke and solar illumination. In addition, radar signals are sensitive to the vegetation volume, structure and moisture content, which would provide information on the vegetation that is complementary to that provided by passive sensors operating at optical wavelengths. Woody biomass and vegetation moisture are in particular essential parameters for predicting fire behavior because they determine, respectively, the fuel loads and the fuel moisture levels.

In October 1994, the Spaceborne Imaging Radar C (SIR-C) provided radar images of Yellowstone at two radar frequencies (C-band, 5.6 cm wavelength and L-band, 24 cm wavelength), and two polarizations (Jordan et al., 1995) (see Figure 1). A few days later, the NASA Jet Propulsion Laboratory multi-frequency polarimetric airborne SAR (AIRSAR) instrument surveyed the same area, providing data over a narrower swath. Similar data had been collected in September 1989 by the same sensor. The AIRSAR data is polarimetric, meaning it measures the full scattering vector of the returned electromagnetic signal as opposed to just a scalar quantity as traditionally done with single-channel radar instruments (Elachi, 1988). Polarimetric information helps interpret radar images acquired at one frequency better and infers geophysical parameters from the radar backscatter values (Ulaby and Elachi, 1990).

Figure 1. False color-composite image of the Yellowstone National Park, Wyoming, acquired by SIR-C SAR in October 1994, after radiometric and geometric compensation for surface topography. Yellowstone Lake is visible as a large dark area at the bottom of the scene. North is on top. The radar is moving from top to bottom, looking to its right, and illuminating a 45-km wide swath.

The objectives of this study were to understand how the SIR-C and AIRSAR radar signals interacted with the burned forests of the Yellowstone National Park, to determine how accurately they could differentiate burned areas from unburned areas and various levels of fire severity, how the results would eventually change with time, radar frequency and polarization, and how they would compare with earlier surveys conducted by other sensors. To validate the results, we utilized visually-interpreted aerial photos of the park from 1988, a classification map produced using Landsat TM imagery from 1988, and the results of limited field surveys.

STUDY SITE

Yellowstone National Park (YNP) is 850,000 ha in size and lies mostly in the northwestern corner of Wyoming and small parts of southwest Montana and southeast Idaho. It consists of large volcanic plateaus of rhyolitic rocks surrounded by mountains of predominantly andesitic rock. The weathered products of andesite produce soils with good fertility and good water holding capacity while rhyolite produces soils that are infertile and dry. Winters are cold, lasting from mid November to mid March. Summers are often dry, usually lasting from July through August. Most of the park is covered with forests of various ages dominated by lodgepole pine (*Pinus contorta*) and Engelmann spruce (*Pica engelmannii*) and subalpine fir (*Abies lasiocarpa)* (Despain, 1990). Other stands include whitebark pine (*Pinus albicaulis*) and Douglas-fir (*Pseudotsuga menziesii*). Lodgepole pine is most common on the rhyolite soils. Andesite soils are mostly covered with Douglas-fir at lower elevations, lodgepole pine or spruce and fir forest at mid and upper elevations and whitebark pine above 2600 m.

Most of the forest is in some stage of succession following natural ecological events, especially fire. The continuous process of fire succession is divided into five recognizable stages based on stand structure (Despain, 1990). In the initial stage, fire ignites from

lightning in old-growth forest of lodgepole pine, Engelmann spruce and subalpine fir, and burns the forest overstory. Seeds protected from the fire in fire-resistant lodgepole pine cones are released after the fire and initiate early succession (Despain et al., 1996). In the first 5 years after the fire (LP0), new seedlings are scarcely noticeable on the forest floor. Forest re-growth is strongly dependent on site conditions and seed banks (Anderson and Romme, 1991). 50-100 years post-burn (LP1), the pines form dense, homogeneous stands, with trees 9-16 m in height. In stage LP2, 150-300 years post-burn, the lodgepole pines thin out, and the precursors of second generation forests of Engelmann spruce and subalpine fir become noticeable on fertile soils. The original trees begin to die in stage LP3, 300 years post-burn, leaving a mixed canopy of lodgepole pine, Engelmann spruce and subalpine fir, with large canopy gaps, a widely diverse understory, and large amounts of dead and flammable materials on the forest floor which render the forest again vulnerable to fire (Renkin and Despain, 1992). The process proceeds quickly on good soils with adequate moisture to reach a dense forest of Engelmann spruce and subalpine fir. On dry, infertile soils, lodgepole pines dominate the understory, resulting instead in a multi-aged lodgepole pine canopy with only a moderate dead and downed fuel component and no spruce-fir understory (stage LP).

METHODS

The SIR-C images of Yellowstone National Park were acquired on October 7, 1994 on orbit 39 of the space shuttle Endeavor. A false-color composite image of the SIR-C data is shown in Figure 1, where the red channel corresponds to the radar brightness of the surface recorded at C-band frequency (5.6-cm wavelength) HH-polarization (horizontal receive and transmit polarization), green is L-band frequency (24-cm wavelength) HH-polarization, blue is L-band HV-polarization (V means vertical polarization). The SIR-C data were rectified and geo-referenced using a USGS 7.5-minute digital elevation model (DEM), at 30 m pixel spacing, in a Universal Transverse Mercator (UTM) projection. The geo-referencing accuracy evaluated on 22 ground control points was better than one SAR pixel (10 m).

Radar images are often processed assuming a flat earth model, which introduces biases in the modeled receiver power at the antenna (Holecz et al., 1994, van Zyl et al., 1993). We applied a set of systematic corrections to remove these errors. The radiometric fidelity was improved to about 1 dB, with residual errors mostly due to a 0.1° uncertainty in roll angle of the SIR-C antenna (Freeman et al., 1995). Even after these corrections, the radar signal was still sensitive to surface topography because the local incidence angle of the radar illumination varies with the surface slope. No systematic corrections are applicable for that effect because it varies with the type of land cover. For forested areas, however, it is reasonable to assume a cosine law dependence of the radar backscatter with the incidence angle (e.g., Bernard and Vidal-Madjar, 1989). Here, the process eliminated all residual variations in radar backscatter due to topography (except for regions of high surface slopes, e.g. mountain peaks, for which the incidence angle of the radar illumination is too large or too low), which in turn validates the cosine-law compensation. The resulting imagery, shown in Figure 1, demonstrates that once surface topography is correctly accounted for in the radiometric correction of the data, the resulting images should be little affected by surface topography, allowing incidence angle independent classification techniques to be applied to the corrected data.

The ability of SIR-C data to detect burned forest was assessed against a map derived from TM imagery. The thematic mapper sensor onboard Landsat 5 provided its first cloud-free image of the 1988 YNP fires on October 2, 1988. The data were geo-rectified and a normalized difference vegetation index was calculated for each pixel. The resultant layer was subjected to an unsupervised classification. Classes that were obviously burned areas were then used as a mask and a second unsupervised classification was run. Post-fire air-photos at a scale of 1:24,000 were independently visually interpreted and cross-verified with field observations conducted at 150 sites. The results of the aerial photographic interpretation were digitized over ten plots, about the size of a U. S Geological Survey (USGS) 7.5 minute topographic quadrangle map, and containing a representative variety and distribution of burn types as well as unburned areas. The results were utilized to combine the 32 satellite image classes into 3 burn categories: canopy burn, mixed burn, and nonforested burn (Ohlen and Despain, manuscript in preparation) (see Figure 2). Surface burn under unburned canopy could not be reliably mapped with Landsat TM.

To classify the SIR-C data, training areas were selected in the false-color composite images based on the color contrast between various types of land cover. Labeling of each training area into a land cover type was performed based on prior classifications of the area (Figure 2) and on an interpretation of the radar scattering characteristics of the training areas (Table 2).

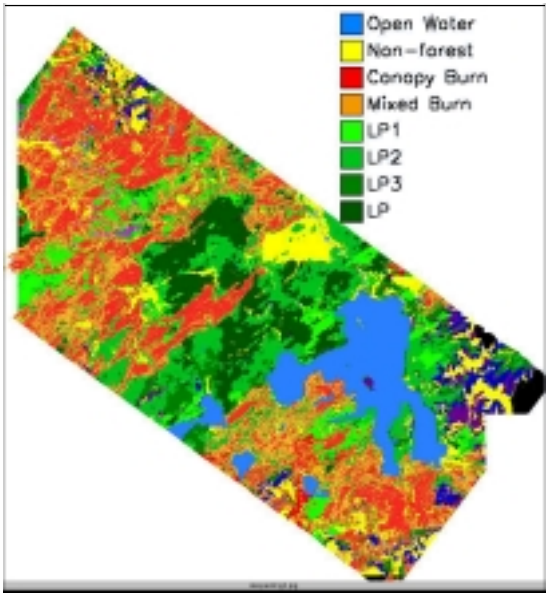

Figure 2. Map of fire severity and vegetation inferred from Landsat TM imagery, aerial photos, and ground surveys over the area imaged by SIR-C SAR in October 1994.

A total of 12 training sites were selected, later regrouped into 8 categories of land cover: 1) open water, 2) nonforested areas; 3) canopy burn; 4) mixed burn; 5) sparse/dry forest; 6) sparse forest; 7) intermediate forest; and 8) dense forest. The multi-channel training statistics from the 12 training sites were then utilized to classify the entire scene using a maximum a posteriori Bayesian classifier (Rignot and Chellappa, 1992). The results are shown in Figure 3.

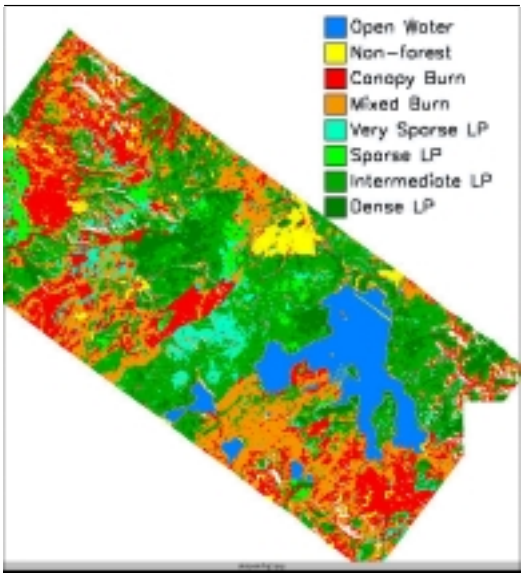

Figure 3. Map of land cover obtained from SIR-C SAR data acquired in October 1994.

Polarimetric radar images were acquired on September 3, 1989 (JPL data reference is CM 4817) and October 10, 1994 (CM 4815 and 4819) by the NASA/JPL airborne AIRSAR instrument. These data were collected along the middle of the SIR-C swath, in the east-west direction, along a 10-km wide swath, with a 10-m pixel spacing, and simultaneously at three radar frequencies: C-, L- and P-band (68 cm). The AIRSAR instrument flies closer to the ground (10 km) than SIR-C (200 km), so its radar illumination angle varies more significantly in the cross-track direction, from about 20° to 70°, compared to being nearly constant about 58.4° in the SIR-C data.

The area shown in Figure 4 is located in the center-left portion of the SIR-C scene (Figure 1). This scene was analyzed to determine the mode of scattering of the radar signals at the three different radar frequencies. The polarimetric signal was decomposed into three canonical forms of radar scattering: 1) single bounce; 2) double bounce; and 3) multiple bounces (volume scattering). The decomposition does not identify specific types of land cover but indicates how the radar signals interact with the surface, which in turn helps in the scientific analysis of the data.

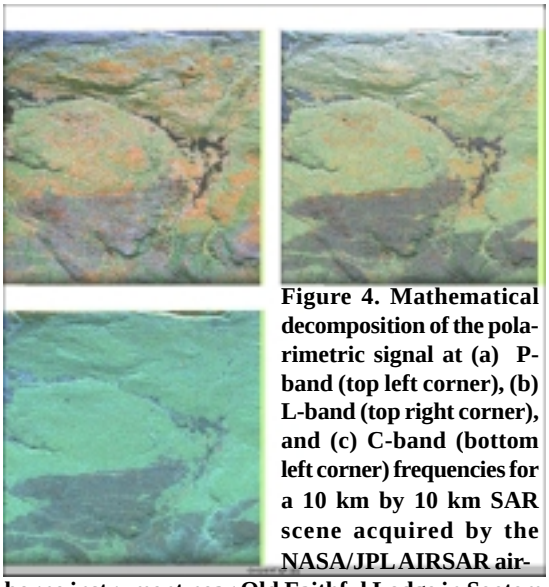

Figure 4. Mathematical decomposition of the polarimetric signal at (a) P-band (top left corner), (b) L-band (top right corner), and (c) C-band (bottom left corner) frequencies for a 10 km by 10 km SAR scene acquired by the NASA/JPL AIRSAR airborne instrument near Old Faithful Lodge in September 1989. Red is double bouncing, green is volume scattering, and blue is single bouncing.

RESULTS

Analysis of Radar Scattering

At C-band, live forest appears green in Figure 4c, meaning volume scattering interactions are dominant.

Burned areas appear blue, meaning single bouncing interactions are dominant. Live forests appear greener at L-band (Figure 4b) than at C-band, indicating that the forest is dense enough at C-band that radar signals bounce off the upper forest canopy. Burned areas also appear more green at L-band than at C-band. This effect cannot be attributed to forest re-growth, which was negligible in 1989, and must be caused by the unconsumed branches. Double bounce reflections (red) are detected in the forest at L-band, and are attributed to scattering from the corner reflectors formed by the trunks and the ground (van Zyl, 1993). Strong double bouncing interactions occur for various reasons, including tall trees, weak attenuation of the radar signals by the canopy, highly reflective ground layers, and low forest density. Here, we attribute the presence of strong double bouncing interactions to a relatively low forest density, low canopy closure, and low understory vegetation of the Yellowstone lodgepole forests growing on poor soils.

At P-band (Figure 4a), volume scattering and double bouncing dominate the radar returns from live forest. Larger patches of forest are colored red at P-band than at L-band, meaning trunk-ground interactions are enhanced at P-band. Burned patches appear blue, but with a stronger green and red components than at L-band. In this case, not only the dead branches but also the dead tree-trunks must play a significant role in radar scattering, otherwise the area should have been predominantly blue (single bouncing from the ground layers).

Burned areas are well separated from unburned areas at P-band HV-polarization, but not at HH- and VV-polarization (Figure 5). At HV-polarization, scattering from the branches dominates, so a lower radar brightness is expected from the burning of the needles and small twigs of the upper canopy and the drying of the larger branches exposed to the fires. At HH- and VV- polarization, the P-band AIRSAR results suggest that the tree-trunks are still efficient scatterers one year after the fire, which implies that they are still holding a lot of moisture. The expected gravimetric moisture content of dead trees is about 9 to 30 percent (Despain, unpublished data; Fosberg et al., 1970), compared to 80 to 100 percent for live trees (Despain, unpublished data; and also Hartford et al., 1991; Chrosciewicz, 1986). The corresponding contrast in dielectric constant is large and should yield detectable differences in radar backscatter at P-band, which we do not see. The reason probably is that it may have taken several years for the dead trees to loose their moisture. If this is the case, we would expect a lower radar backscatter from dead forests several years after the fire. This is indeed what is being observed in the P-band HH data collected by AIRSAR in 1994. In the 1994 P-band imagery, burned areas are distinguishable from non-burned areas because their radar brightness has become lower.

The change in radar brightness with time is different at C-band. In the 1989 imagery, burned areas are easily identified at all polarizations, which we attribute to the burning of the upper forest canopy (needles and twigs) which scattering models indicate to be the main scattering centers at that frequency. Most of the understory vegetation has been consumed by the fire and the forest floor has a relatively smooth surface so the radar returns from burned forests are low. In the 1994 imagery, however, the burned areas are no longer separated from non-burned areas at C-band HH and VV polarization (Figure 5). The situation is therefore opposite to that observed with the P-band data. We attribute the strong scattering from burned areas in the 1994 image to vegetation re-growth developing on the forest floor (grasses, shrubs, seedlings). C-band signals are known to be sensitive to short vegetation and low vegetation biomass, and also saturate quickly with increasing biomass. Burned areas are still visible at HV-polarization because the ground layers have much less influence on the radar signals at that polarization for which radar signals are typically dominated by scattering from the forest canopy.

The L-band data correspond to a scattering behavior intermediate between C-band and P-band data. Burned areas are well distinguished in both the 1989 and 1994 data at like polarization. At HV-polarization, all frequencies showed a consistently large difference in backscatter between burn and non burn, but the largest difference is recorded at L-band, which means that L-band frequency is probably the most reliable of all three radar frequencies for mapping burned areas.

To conclude, we find that different radar frequencies respond differently to forested areas affected by a fire, and that behavior changes with time and seems to provide useful information on forest recovery and on changes in fuel moisture levels. These examples hence illustrate imaging radars' significant abilities to detect burned areas, but also monitor forest recovery.

Landsat TM Fire Severity Map

The results of the comparison between the Landsat TM classification and a set of 10 areas mapped using aerial photos Despain et al., 1989) is summarized in the con-

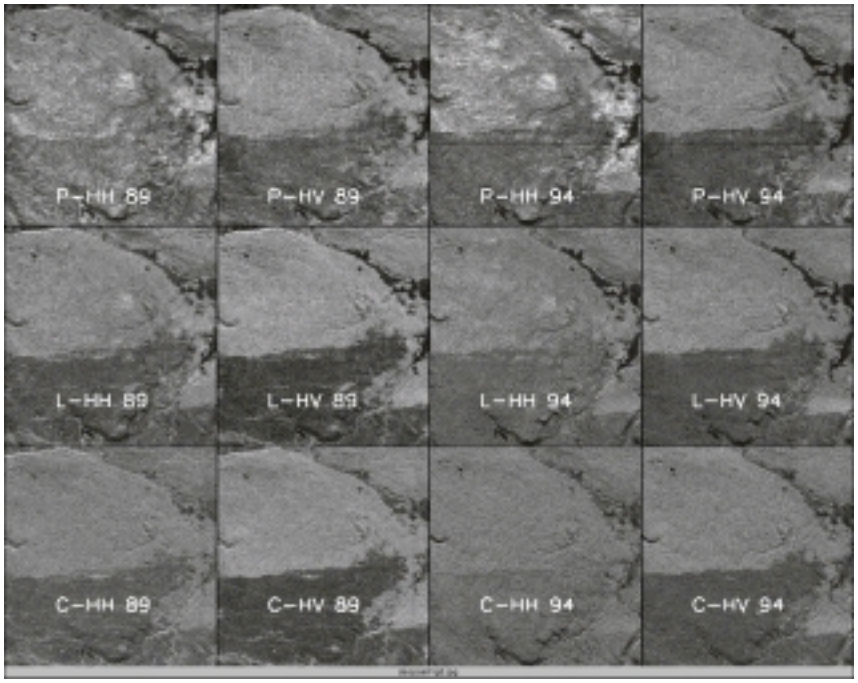

Figure 5. Radar brightness of the Yellowstone National Park acquired in September 1989 (first two columns) and in October 1994 (last two columns) by the NASA/JPL AIRSAR instrument at HH polarization (column 1 and 3), and HV polarization (column 2 and 4), with P-band frequency (first row), L-band (second row) and C-band (last row). The area of interest is near the center of the SIR-C image shown in Figure 1.

fusion matrix in Table 1. The kappa coefficient of agreement for the entire classification (Rosenfield and Litzpatrick-Lins, 1986) is 82.5 percent. The category "Other" listed in Table 1 includes areas of overlap due to the difference in resolution between the aerial photos and the satellite imagery, shadow areas, areas of steep slope, unburned nonforested areas, and areas of surface burn (Despain et al., 1989). The corresponding map of fire severity is shown in Figure 3. In this map, we regrouped under the same color nonforested areas that burned in 1988 and unburned nonforested areas (shrublands, grasslands, and meadows). Unburned forests are separated into 6 major classes: 4 successional stages of lodgepole pine forests, stands dominated by Douglas-fir, and stands dominated by white bark pine. These unburned categories were not obtained from the Landsat TM classification but from a vegetation map assembled from visually-interpreted aerial photos taken in 1969-72 (Despain, unpublished data). The original vegetation map comprised 42 classes of land cover which we regrouped into only 6 major classes of land cover to simplify the presentation and the discussion.

σ^{o}_{HH} L	σ^{o}_{HV} L	σ^{o}_{HH} C	Type of land cover
-32.8	-39.4	-26.1	Open water
-21.7	-30.3	-18.0	Nonforested
-16.5	-25.5	-17.3	Canopy Burn, dense
-13.4	-23.0	-14.3	Canopy Burn, sparse
-15.2	-23.5	-15.8	Mixed Burn
-14.9	-23.4	-17.2	Very Sparse, dry forest
-12.8	-21.5	-16.5	Sparse, dry forest
-14.1	-20.7	-16.1	Intermediate forest
-12.8	-19.9	-16.2	Dense forest

Table 1. Radar backscatter characteristics of several types of land cover at L-band HH (σ^{o}L), L-band HV (σ^{o}_{HV} L) and C-band HH (σ^{o}_{HH} C) expressed in dB used for classification of the SIR-C data into land cover types (Figure 3).

Land Cover Classification with SIR-C

Burned areas appear red in Figure 1 because C-band HH data does not separate the burn, as seen with the AIRSAR data (Table 2). Areas colored yellow in Figure 1 (north-west sector) correspond to canopy burn in sparse, dry forest developing on infertile soils of sand and gravel with little forest floor vegetation. The western portion of that sector is colored bright green and corresponds to the unburned portion of the sparse, dry forest.

Category	Canopy Burn	Mixed Burn	Nonforest Burn	Unburned	Other	K
Canopy Burn	90	0	0	5	5	87
Mixed Burn	0	90	5	0	5	87
Nonforest Burn	0	5	80	10	5	73
Unburned Forest	0	0	5	85	10	80

Table 2. Confusion Matrix of the Landsat TM data and values of the kappa coefficient of agreement for each class and for the entire classification. Kappa Coefficient = 82.5 percent.

A smaller stand of similar radar characteristics was present in the northern portion of the AIRSAR scene and showed significant double bounce scattering at both P-, L- and even C-band. We visited that area and found a sparse forest, with a few large dead standing trees, no understory vegetation, and a smooth forest floor. This configuration favors double bounce interactions and illustrates that dead tree trunks can be significant sources of radar backscatter after a fire. This conclusion is also supported by the analysis of radar scattering at the P-band frequency.

The accuracy of the SIR-C classification (Figure 3) can be seen using Landsat TM classification (Figure 2) as a reference since its comparison with the aerial photos showed a high classification accuracy. Burned areas appear to be mapped with a high degree of accuracy. The agreement between the different levels of fire severity is less, as discussed below.

Commission errors include patches of live forest in the highest mountain ranges at the corners of the scene. These forests comprise a mixture of whitebark pine trees and nonforest, therefore of very low crown biomass, explaining the possible confusion with forest burn. Isolated wildland fires are unlikely at these high-elevations so the error could easily be dismissed by a human interpreter.

Omission errors include several patches of mixed burn located in the north-east sector of the scene, north of an easily recognized, large, triangular-shape meadow. Forest re-growth is significant at that location, with tree seedling reaching a couple of meters, which may explain why the SIR-C data are confusing them with unburned forest. In addition, this part of the scene has a 1 dB calibration uncertainty due to uncertain knowledge of the roll angle of the antenna. The radar signal is brighter in that part of the image, including in live forests, although no major difference in vegetation cover exist in that area, which means that the radiometric correction of the data is not entirely reliable.

Very sparse and dry forest exhibits radar characteristics similar to that of mixed burn (Table 2). Without ancillary information, or multi-date radar images, it would have been difficult from the SIR-C data alone to infer that this forest had not been affected by a fire. No recent fires affected this area. Most of the forest lays above the 2600 m contour line where air temperatures are colder on average than in the rest of the park, and where soil conditions were reportedly drier than average in October 1994. Numerous whitebark pine trees are also present in this forest, giving the canopy slightly different characteristics. We therefore attribute the lower L-band HV brightness of this region to lower moisture levels, combined with the presence of other tree species besides lodgepole pine. The classes of live forest outlined by SIR-C were poorly correlated with forest successional stages. The correlation coefficient was 10 percent. The radar data may be more influenced by stand densities than a human interpreter looking for the outlines of even-aged stands. Neighboring stands of similar age may vary widely in terms of canopy structure and fresh crown biomass and are therefore unlikely to provide similar radar brightness. We therefore attribute most of the differences in backscatter between the different classes of live forests to various levels of crown biomass and vegetation moisture.

DISCUSSION

The comparison of the SIR-C and Landsat TM classification showed a reasonable level of agreement in terms of the total area affected by the fire but also significant differences in areas of mixed burn and canopy burn. These differences are however expected and are the product of forest recovery in the years after the fire and loss of needles by trees killed by the fire but still retained their needles in the TM image. The SIR-C data seem to reveal differences in crown biomass, vegetation moisture and structure of the forest, which is complementary to the information provided by Landsat on the amount of photosynthetically active vegetation.

Landsat TM data probably identify live vegetation more reliably than imaging radar data but the radar data are potentially more useful for predicting the fuel loads and the fuel moisture levels of the forest, which are essential inputs for models of fire behavior and growth prediction.

Initial re-growth proceeds slowly at the beginning but may then reach 30 cm/yr about 5-6 years after the fire (Despain, unpublished data). New seedlings had in 1994 a height ranging from a few centimeters in areas of infertile dry soils to 1 or 1.5 m on good soils. Crown biomass of 1.5 m trees should be about 360g (Brown, 1978). Many burned stands had densities of approximately 1 seedling per square meter which would equal 0.4 kg/m^2. We estimate the crown biomass of mature live forest to be about 1-2 kg/m^2 while mixed burn stands will have less depending on how many crown burned (Despain, unpublished data). Further field verification of these preliminary results are necessary to determine the sensitivity of SIR-C data to forest regrowth.

The results of this study showed good potential for imaging radar to map burned areas on a single date. The results would probably improve significantly by using multi-date imagery and change detection techniques because the changes in land cover type would be recorded more directly. Cross-polarized radar channels provide the best means of mapping burned areas, but if multi-date imagery is available multi-channel data may not be necessary and any single channel system should be able to detect biomass burning. The potential advantage of multi-channel data is to infer the amount of woody biomass and its distribution along the forest profile (meaning trunk biomass versus branch biomass and leaf biomass), which is something difficult to achieve using single-channel data, along with some information on the moisture levels of the vegetation through the estimation of their dielectric constant.

The SIR-C survey of Yellowstone illustrates the potential for the radar technique to the study of forest fire and forest monitoring. More studies are needed to understand in more detail the sensitivity of the radar signals to the forest fuel loads and fuel moisture, which requires in-situ data collected at the time of passage of the radar instrument.

Several space-borne SARs are currently orbiting the earth but all operate at a single channel. A single-channel radar system is sufficient to obtain basic information on biomass burning, such as the location and spatial extent of the fires. Examples of such applications of the radar technique have already been shown using ERS-1 SAR in Alaska (Kasischke et al., 1995) and Africa (Malingreau, 1996). Those data were typically analyzed a few months after data acquisition because of the time needed to downlink the data, send them to the archive center, order processing, distribute the products to the investigators and analyze the data; but there is no major obstacles to having this technology deliver data products in key areas within a few hours of the data acquisition.

CONCLUSIONS

The radar images of the Yellowstone National Park demonstrate the abilities of imaging radar to detect burned areas and provide information on forest recovery in the years following fire disturbance. The results compare well with earlier surveys conducted in 1988 using optical instruments. Various levels of fire severity can be detected by radar, and the radar data are sensitive to the forest fuel loads and fuel moisture levels. Quantitative verification of these results will require detailed forest inventories, which have not yet been done.

ACKNOWLEDGEMENTS

This work was partly carried out at the Jet Propulsion Laboratory, California Institute of Technology, under a contract with the National Aeronautics and Space Administration. The authors would like to thank all the people at the Jet Propulsion Laboratory involved with the processing and generation of the SIR-C SAR products.

REFERENCES

Anderson, J. E., and Romme, W. H. (1991). Initial floristics in lodgepole pine (*Pinus contorta)* forests following the 1988 Yellowstone Fires, Int. J. Wildland Fire, 1:119-124.

Beaudoin, A. and 9 others. (1994). Retrieval of forest biomass from SAR data, Int. J. Rem. Sens., 15:2777-2796.

Bernard, R., and Vidal-Madjar, D. (1989). C-band radar cross section of the Guyana rain forest: possible use as a reference target for spaceborne radars, Rem. Sens. Environ., 27:25-36.

Christensen, N. L. and 11 others. (1989). Interpreting the Yellowstone fires of 1988, BioScience, 39:678-685.

Chrosciewicz, Z. (1986). Foliar moisture content variations in four coniferous tree species of central Alberta, Can. J. .For. Res., 16:157-162.

Despain, D. G., Rodman, A., Schullery, P. and Shovic, H. (1989). Burned area survey of Yellowstone National Park: the fires of 1988, Yellowstone National Park, Wyoming, U. S. Department of the Interior, National Park Service, Yellowstone National Park, 14p.

Despain, D. (1990). Yellowstone's vegetation: the consequences of history and environment in a natural setting,, Roberts Rinehart Inc., New York.

Despain, D. G., Clark, D. L., and Reardon, J. J. (1996). Simulation of crown fire effects on canopy seed bank in lodgepole pine, Int. J. Wildland Fire,, In press.

Elachi, C. (1988). Spaceborne radar remote sensing: applications and techniques, IEEE Press, The Institute of Electrical and Electronics Engineers, New York, NY, 255 pp.

Fosberg, M. A., Lancaster, J. W., Schroeder, M. J. (1970). Fuel moisture response: Drying relationships under standard and field conditions, Forest Science, 16:121-128.

Freeman, A. and 8 others. (1995). SIR-C data quality and calibration results, IEEE Trans. Geosc. Rem. Sens., 33:848-857.

Hartford, R. A. and Rothermel, R. C. (1991). Fuel moisture as measured and predicted during the 1988 fires in Yellowstone Park, Intermountain Research Station Research Note INT-396. Intermountain Research Station, Ogden Utah. 7p.

Holecz, F., Meier, E., Piesbergen, J., Nuesch, D. and Moreira, J. (1994). Rigorous derivation of the backscattering coefficient, IEEE Trans. Geosc. Rem. Sens. Newsletter, 92:6-14.

Jordan, R. L., Huneycutt, B. L., and Werner, M. (1995). The SIR-C/X-SAR Synthetic Aperture Radar System, IEEE Trans. Geosc. Rem. Sens., 33:829-839.

Renkin, R. A., and Despain, D. G. (1992). Fuel moisture, forest type, and lightning-caused fire in Yellowstone National Park, Can. J. For. Res., 22:37-45.

Rignot, E. and Chellappa, R. (1992). Segmentation of polarimetric synthetic aperture radar data, IEEE Trans. Imag. Proc., 1:281-300.

Romme, W. H. and Despain, D. G. (1989a). Historical perspective on the Yellowstone fires of 1988, BioScience, 39:695-699.

Romme, W. H. and Despain, D. G. (1989b). The long history of fire in the Greater Yellowstone Ecosystem, Western Wildlands, 15:10-17.

Rosenfield, G. H. and Fitzpatrick-Lins, K. (1986). A coefficient of agreement as a measure of thematic classification accuracy, Photogrammetric Engineering and Remote Sensing, 52:223-227.

Rothermel, R. C., Hartford, R. A. and Chase, C. H. (1994). Fire growth maps for the 1988 Greater Yellowstone Area Fires, U. S. Department of Agriculture, Intermountain Research Station, Ogden Utah, Tech. Rep. INT-304., 1994.

Schullery, P. (1989). Yellowstone fires: A preliminary report, Northwest Science, 63:44-54.

Stofan, E. R. and 7 others. (1995). Overview of results of Spaceborne Imaging Radar-C, X-band synthetic aperture radar (SIR-C/X-SAR), IEEE Trans. Geosc. Rem. Sens., 33:817-828.

Ulaby, F. T., and Elachi, C. (1990). Radar Polarimetry for Geoscience Applications, Artech House, Norwood, MA.

van Zyl, J. J., Chapman, B. D. and Dubois, P. (1993). The effect of topography on SAR calibration, IEEE Trans. Geosc. Rem. Sens., 31:1036-1043.

van Zyl, J. J. (1993). The effect of topography on radar scattering from vegetated areas, IEEE Trans. Geosc. Rem. Sens., 31:153-160.

van Zyl, J. J. (1992). Application of Cloude's target decomposition theorem to polarimetric imaging radar data, Proc. SPIE, 1748:184-191.

Waring, R. H. and 7 others. (1995). Biologists toolbox - imaging radar for ecosystem studies, BioScience, 45:715-723.